A Novel Method Utilizing Trapezoidal Voltage to Compensate for Inverter Nonlinearity

Yongsoon Park, *Student Member, IEEE*, and Seung-Ki Sul, *Fellow, IEEE*

Abstract—The nonlinearity of an inverter could be regarded as the output distortions of the inverter. In this paper, voltages in a trapezoidal form were utilized to compensate for the nonlinearity of an inverter. Undesirable harmonic distortions in the overall system were mitigated through the modulating shape of the trapezoidal voltage. For trapezoidal modulation, a dedicated modulator was designed to facilitate adaptive compensation for a wide operating range. The compensation effects from the proposed method were examined in a practical system, in which a permanent magnet synchronous motor (PMSM) was driven without any position sensor. Additionally, it was shown that the proposed method could enhance the sensorless control of the PMSM by reducing the output distortions of the inverter.

Index Terms—Inverter nonlinearity, permanent magnet synchronous motor (PMSM), sensorless control, trapezoidal voltage.

I. INTRODUCTION

THE nonlinearity of an inverter can be considered as the voltage differences between the voltage references and actual outputs of the voltage source inverter (VSI). However, in a sensorless control system with a permanent magnet synchronous motor (PMSM), voltage references are used instead of actual voltages in order to estimate the rotor angle for practical reasons [1]–[3]. Hence, the inverter nonlinearity, which causes the voltage differences, can affect the performance of the sensorless control system.

Moreover, the harmonic distortions in the output currents are mostly caused by the inverter nonlinearity, which are mainly distributed in the low-order harmonics. Thus, the problem may be worse in a sensorless control system, where the estimated angle can be equivalently expressed as the low-pass filtering (LPF) of the actual angle [1], [2]. Then, the high-order harmonics can be more easily attenuated through the LPF. However, if the low-order harmonics in the voltage reference are not filtered out sufficiently, they can be visibly reflected on the estimated angle and speed. This can deteriorate the efficacy and stability of the sensorless control system.

The nonlinearity of an inverter is caused by practical characteristics including preset dead time, switching delays, para-

sitic capacitances, and on-state voltages in the inverter. A lot of research has been done for the last few decades, which has focused on how to compensate for each factor due to the nonlinearity [4]–[9]. However, since those compensations are based on limited data sampled only under certain operating conditions, it is difficult to ensure their effectiveness for all operating conditions.

Meanwhile, other attempts have been carried out using the disturbance observer [13]–[16]. In these methods, the inverter nonlinearity is regarded as the disturbances to be mitigated. The observer, used to estimate the disturbance voltages, is expected to be effective for a wide operating range. However, electrical parameters, which can vary depending on the circumstances, are used to design the observer. That is, the performance of the observer would be limited by the operating conditions, contrary to expectations. Moreover, the rotor angle, which is also crucial for the observer design, can be inaccurate in the sensorless control system.

In this paper, a novel method was proposed to compensate for the low-order harmonics from the inverter nonlinearity. The proposed method is similar to the observer-based method, in that the nonlinearity is regarded as voltage distortions. However, the proposed compensation method can adapt to varying operating conditions without the aid of any observers. Namely, the physical parameters are not necessary for the adaptation in the proposed method. This can contribute by improving the robustness of the proposed method for various operating conditions. Its effectiveness is discussed with experimental results in a sensorless control system, where more diverse effects from the nonlinearity can be observed.

II. COMPENSATION VOLTAGE

Software is preferable to hardware if any modification is necessary in the commission stage or during driving. The software for digital control corresponds to source code, which is executed per one sampling period in a digital signal processor (DSP). Thus, if a software-based compensation is required, the inverter distortions, which are averaged for one sampling period, should be considered. An averaged model of the inverter was obtained stage by stage (see Fig. 1).

At first, some inverter properties, like the on-state voltages and parasitic capacitances, can be isolated conceptually from the original inverter in Fig. 1(a). Then, the inverter itself is described with ideal switches [see Fig. 1(b)], while the nonlinear properties are separated as $d(i_{as})$, $d(i_{bs})$, and $d(i_{cs})$. Even though the properties of the switches are ideal, the turn-on and turn-off of each switch can still be distorted by the temporal nonlinearity from the dead times and switching delays.
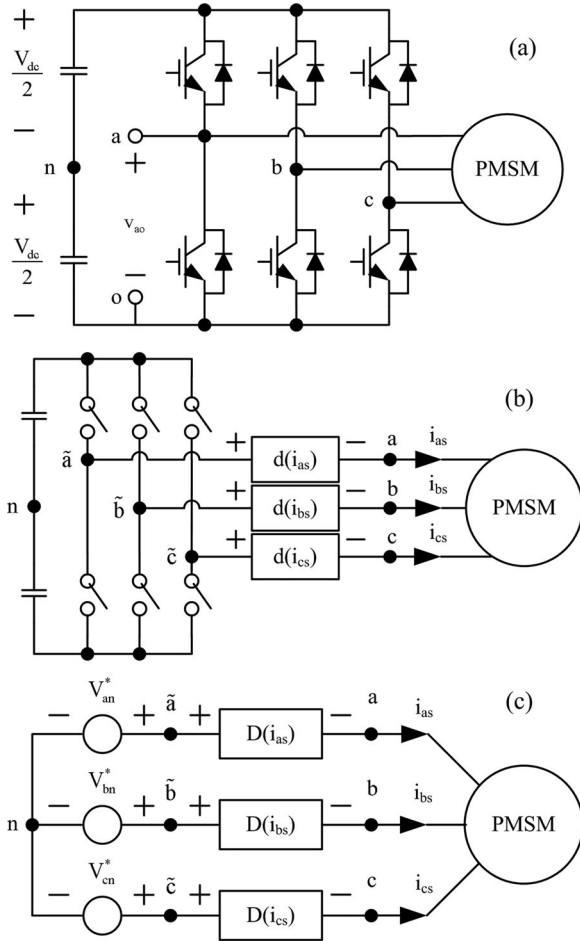
Fig. 1. Modeling of an inverter: (a) original inverter, (b) inverter with ideal switches, and (c) averaged inverter model per one sampling period.

When the circuit in Fig. 1(b) is averaged for one sampling period, it becomes possible to consider the temporal distortions. These distortions can also be separated from the inverter and are reflected on the nonlinear loads, $D(i_{as})$, $D(i_{bs})$, and $D(i_{cs})$ [see Fig. 1(c)]. Since the inverter nonlinearity is entirely separated as the nonlinear loads, pole voltages can be synthesized equal to their references in the circuit in Fig. 1(c). This is summarized in (1). Hereafter, the superscript "∗" denotes the reference value

$$V_{\tilde{a}n} = V_{an}^*, \quad V_{\tilde{b}n} = V_{bn}^*, \quad V_{\tilde{c}n} = V_{cn}^* \quad (1)$$

where $V_{\tilde{a}n}$ is the voltage from n to $\tilde{a}$.

The compensation principle is clarified with Figs. 1(c) and 2. The perfect compensation is to achieve (2) in the circuit in Fig. 1(c) through the mechanism depicted in Fig. 2

$$\begin{cases} V_{a\tilde{a}} = -D(i_{as}) + V_{inv}^a = 0 \\ V_{b\tilde{b}} = -D(i_{bs}) + V_{inv}^b = 0 \\ V_{c\tilde{c}} = -D(i_{cs}) + V_{inv}^c = 0 \end{cases} \quad (2)$$

where V_{inv}^a indicates the compensation voltage of the a-phase.

Based on (1) and (2), the ideal compensation can be described with (3), which means that there are no differences between the
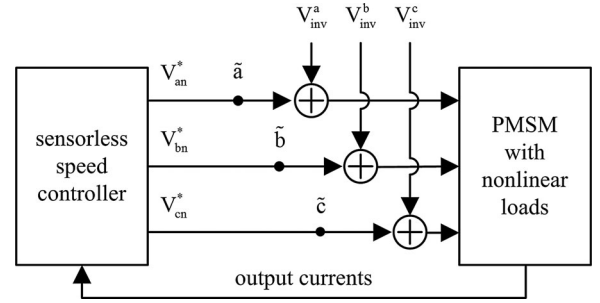

Fig. 2. Addition of compensation voltages.

voltage references and actual voltages of the PMSM:

$$\begin{cases} V_{an} = V_{a\tilde{a}} + V_{\tilde{a}n} = V_{an}^* \\ V_{bn} = V_{b\tilde{b}} + V_{\tilde{b}n} = V_{bn}^* \\ V_{cn} = V_{c\tilde{c}} + V_{\tilde{c}n} = V_{cn}^*. \end{cases} \quad (3)$$

Therefore, it is crucial to determine how to accurately obtain the compensation voltages, V_{inv}^a, V_{inv}^b, and V_{inv}^c in Fig. 2.

A. Sign Definition of the Distorted Voltage by the Inverter

To deal with the distorted voltages, depicted in Fig. 1(c) as $D(i_{as})$, $D(i_{bs})$, and $D(i_{cs})$, their signs with respect to the currents flowing into them should be defined first. The following discusses how each factor of the nonlinearity affects the sign definition.

To use the a-phase as an example, the terminal voltage v_{ao} is defined in Fig. 1(a), and its waveform is displayed in Fig. 3. In general, the dead times are inserted as depicted in Fig. 3, where only the turn-on instant of each active switch in the leg is delayed by T_d from the original instant. However, the actual voltage waveform can be further distorted by freewheeling diodes depending on the output current as classified in Fig. 3. The volt-second distortion due to the dead time occupying "Y" in Fig. 3 can be a loss or gain of the volt-second depending on whether the actual interval T_a is increased or decreased from its reference, T_a^* [8]–[11]. Then, the actual outputs could be expressed in terms of the volt-second as shown in

$$\begin{cases} V_{dc}T_a = V_{dc}(T_a^* - T_d), & i_{as} > 0 \\ V_{dc}T_a = V_{dc}(T_a^* + T_d), & i_{as} < 0. \end{cases} \quad (4)$$

If every part of (4) is divided by one switching period, the volt-seconds are transformed into the voltages of (5), where the bar "-" over a variable indicates the average of that, and the voltage distorted by the dead time is denoted by V_d

$$\begin{cases} \bar{v}_{ao} = \bar{v}_{ao}^* - V_d, & i_{as} > 0 \\ \bar{v}_{ao} = \bar{v}_{ao}^* + V_d, & i_{as} < 0. \end{cases} \quad (5)$$

In order to output the actual voltage of $\bar{v}_{ao}$ correctly, the voltage reference of $\bar{v}_{ao}^*$ must reflect the distorted voltage additionally. After considering (5), it can be concluded that the distorted voltage seems to be the voltage drop of a hypothetical resistor. Namely, the sign of the distorted voltage varies depending on the flowing current like that of a resistor when the voltage reference is considered as a supplying voltage source. This sign
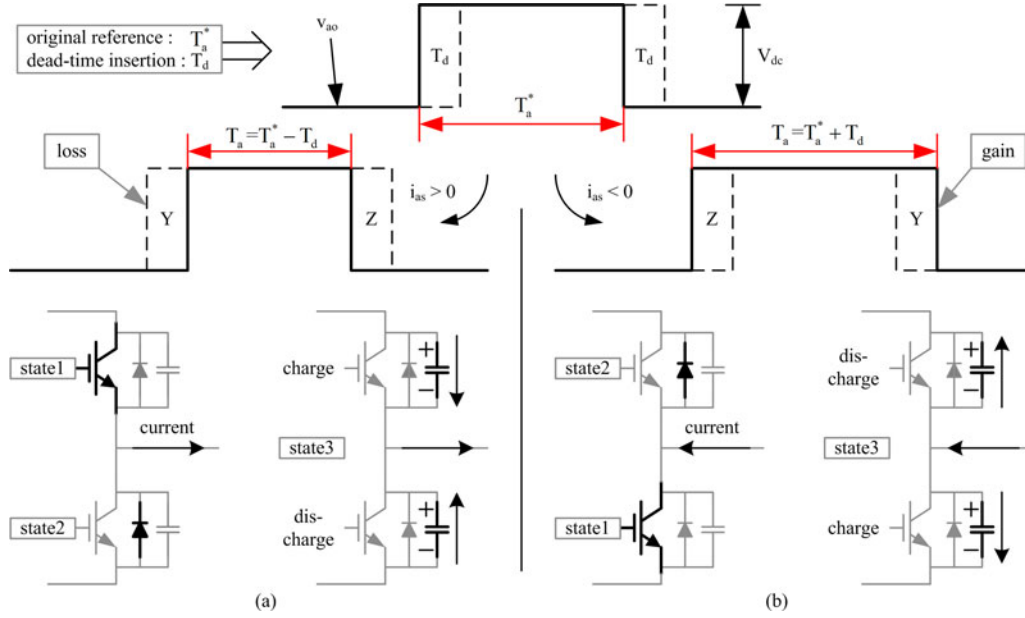
Fig. 3.   Influences by dead times and parasitic capacitances: (a) positive output current and (b) negative output current.
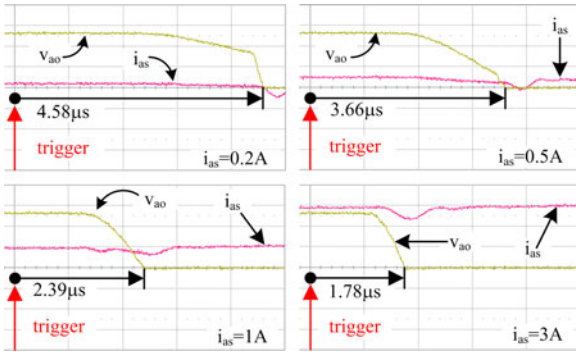

Fig. 4.   Variation of the terminal voltage according to the current magnitude at turn-off instant: v_{ao} (200 V/div, center 0 V), i_{as} (1 A/div, center 0 A), time (1 μs/div).

definition can be maintained even though the on-state voltage drops from the active switches are merged into V_d, since the switches are actual passive elements.

The distortion by parasitic capacitances can also be explained through the regions indicated by "Z" in Fig. 3. The current path is instantly changed from "state1" to "state2" at the start of "Z" if the influence of the parasitic capacitances can be negligible. Otherwise, "state3" can conspicuously affect the output voltage waveform during "Z." That is, the solid boundary of "Z" approaches to the dashed boundary of "Z" [12]. This point can be understood through Fig. 4.

The terminal voltage at turn-off was captured in a prototype inverter set, where the dc-link voltage is about 530 V, and the flowing current to the output terminal is regulated as a dc value. As shown in Fig. 4, the time for the terminal voltage v_{ao} to reach 0 V was different depending on the current, because the charging and discharging currents of the parasitic capacitances in "state3" of Fig. 3(a) were different at each case in Fig. 4. When the influence of "state3" became dominant, the settling time increased. This means increment of the volt-second distortion

from the parasitic capacitances. The settling time could be larger than the preset dead time of 3 μs at some cases, since delays between the control signal and the actual gating signal were also included in the specified times in Fig. 4.

The distorted voltage from the dead time can be offset by the distorted voltage from the parasitic capacitances, because the sign of the distorted voltage is opposite to each other. However, the total sum of the volt-second distortions can scarcely be negative in a practical system since the distortion that occurred in "Z" is almost always smaller than that in "Y." Therefore, for the voltage distorted by the inverter, its overall sign is defined like in (6) combined with Fig. 1(c)

$$\begin{cases} D(i_{xs}) > 0, & \text{if } i_{xs} > 0 \\ D(i_{xs}) < 0, & \text{if } i_{xs} < 0 \end{cases} \tag{6}$$

where the phase "x" can be a, b, or c.

B. Distorted Voltage Under the Stationary Condition

The back electromotive force (EMF) of a PMSM is zero under the stationary condition. Furthermore, voltage drops on the inductances of the PMSM can also be ignored in the average sense when the currents are regulated as dc values by a pulsewidth modulation (PWM) of VSI. Under these conditions, the PMSM can be modeled as a three-phase resistive load, and the voltage reference would be in phase with the output current. Then, if the output currents are regulated as (7) in the stationary d–q reference frame, they can be transformed into (8) through the inverse Clarke transformation

$$i_{ds}^s > 0, \quad i_{qs}^s = 0 \tag{7}$$

$$\begin{bmatrix} i_{as} \\ i_{bs} \\ i_{cs} \end{bmatrix} = \begin{bmatrix} 1 & 0 \\ -1/2 & \sqrt{3}/2 \\ -1/2 & -\sqrt{3}/2 \end{bmatrix} \begin{bmatrix} i_{ds}^s \\ i_{qs}^s \end{bmatrix} = \begin{bmatrix} i_{ds}^s \\ -i_{ds}^s/2 \\ -i_{ds}^s/2 \end{bmatrix} \tag{8}$$

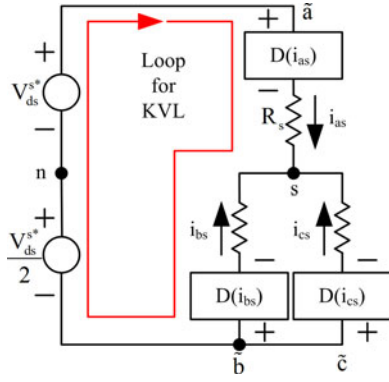where superscript "s" means the stationary d–q reference frame.

Fig. 5.   Driving circuit of a PMSM under the stationary condition.

Fig. 6.   Distorted voltage under the stationary condition.

Fig. 7.   Shape of the compensation voltage (trapezoidal voltage).

In the similar manner, the voltage references for each phase, which are in phase with the currents, can be obtained as (10) from (9)

$$v_{ds}^{s*} > 0, \qquad v_{qs}^{s*} = 0 \qquad (9)$$

$$v_{as}^* = v_{ds}^{s*}, \qquad v_{bs}^* = v_{cs}^* = \frac{-v_{ds}^{s*}}{2}. \qquad (10)$$

Based on (10) and Fig. 1(c), the equivalent circuit of the PMSM can be drawn like Fig. 5 under the stationary condition. Applying Kirchoff's voltage law (KVL) to the loop in Fig. 5, the voltage equation can be derived as

$$-\frac{3}{2}V_{ds}^{s*} + D(i_{as}) + R_s i_{as} - R_s i_{bs} - D(i_{bs}) = 0 \qquad (11)$$

where R_s is the equivalent resistance, which includes the resistances of the PMSM and switch modules.

For simple discussion, if the distortion from the dead time is only considered, the distorted voltage can be assumed as a constant V_{dead} and (6) can be simplified into

$$\begin{cases} D(i_{xs}) = V_{\text{dead}}, & \text{if } i_{xs} > 0 \\ D(i_{xs}) = -V_{\text{dead}}, & \text{if } i_{xs} < 0 \end{cases}, \quad \text{when } V_{\text{dead}} \geq 0 \qquad (12)$$

where the phase "x" can be a, b, or c.

If each phase current in (11) is substituted by the d-axis current according to (8), and the functions of D(-) in (11) are replaced with respect to V_{dead} of (12), the distorted voltage can be derived as

$$V_{\text{dead}} = \frac{3}{4} \cdot (V_{ds}^{s*} - R_s \cdot i_{ds}^s). \qquad (13)$$

The practical system, which is specified in Section III-A, was considered to calculate the distorted voltage, V_{dead} in (13). In that system, the output currents were controlled to satisfy (7) under the stationary condition, and the d-axis voltage references were accordingly sampled, which corresponds to V_{samp} in Fig. 6. To acquire the distorted voltage through (13), the equivalent resistance R_s should be computed first, which corresponds to the slope of V_{samp}.

Because the sole origin of V_{dead} is assumed as the dead time at (12), the resistance should be computed in the large current region to exclude the effects of the parasitic capacitances. If R_s is compute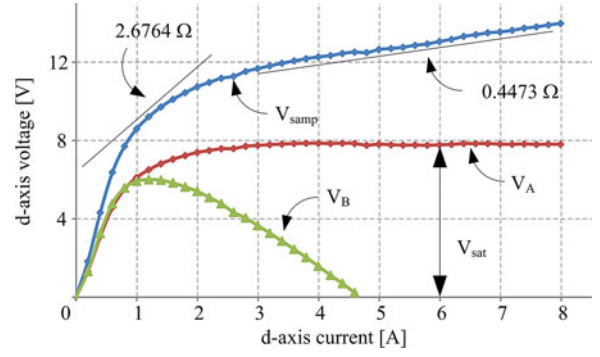d as 2.6764 Ω in the small current region, the distorted voltage is obtained by (13) as V_B in Fig.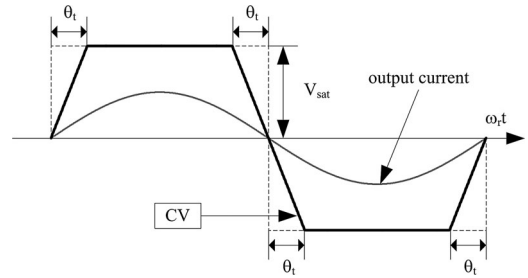 6, which is contrary to the assumption of a constant V_{dead}. By contrast, the distorted voltage can be obtained as V_A with the resistance of 0.4473 Ω in the large current region, which is almost saturated as 7.88 V. This V_A in Fig. 6 would be useful for compensation of the inverter nonlinearity.

C. Shape of the Compensation Voltage (CV)

A sort of distorted voltage in Fig. 6 has already been exploited for the compensation to reflect the present state of an inverter. One method is only using the saturated voltage [4], V_{sat} in Fig. 6. This method exhibits its effectiveness when the magnitude and frequency of the output current are large enough. However, as shown in V_A of Fig. 6, the distorted voltage can vary in the small-current region. To compensate for this deficiency, several methods were proposed [5], [7], [17]. One of them is to use a look-up table [5], storing the entire data of V_A up to saturation in Fig. 6.

In this paper, the trapezoidal voltage, CV in Fig. 7, was utilized for the compensation voltage in Fig. 2, whose height was determined from V_{sat} in Fig. 6. This voltage should be in phase with the output current as indicated by (6). Especially, the trapezoidal angle θ_t in Fig. 7 can be adjusted for the suitable compensation. Depending on θ_t, the proposed method could be similar to each of the conventional methods in [4] and [5].

It could be discussed in the frequency domain what the modulation of the trapezoidal angle means, based on the Fourier coefficients of the trapezoid. Their magnitudes are depicted in Fig. 8 according to θ_t when V_{sat} is unity. Up to 30°, the fundamental only decreased by 4.5% while the other harmonics, 5th, 7th, 11th, and 13th, changed drastically. This indicates that
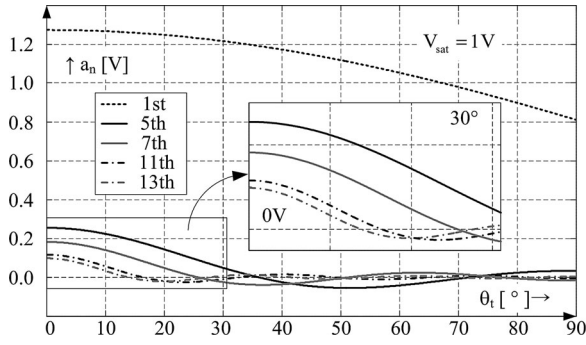
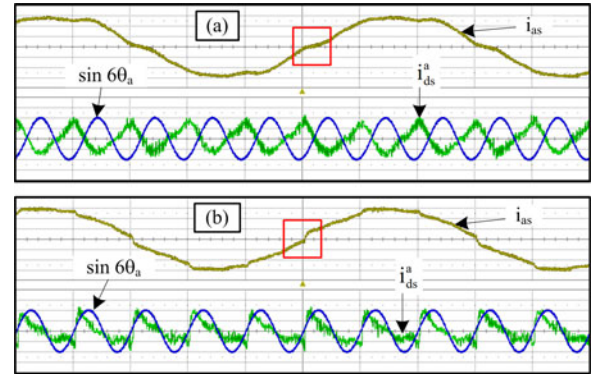Fig. 8. Fourier coefficients of the trapezoid according to θ_t.

Fig. 9. Harmonics in the output current depending on the harmonics of the compensation voltage, 500 r/min, no load: (a) insufficient compensation voltage and (b) excessive compensation voltage—i_{as} (0.5 A/div, center 0 A), $\sin6\theta_a$ (0.5/div, center 0), i_{ds}^a (0.1 A/div, center 0 A), time (10 ms/div).

the low-order harmonics of the trapezoidal voltage, except for the fundamental, can be modulated by adjusting θ_t. By contrast, in the conventional methods, ratios of the low-order harmonics to the fundamental can be considered as being fixed once the compensation voltage is determined. This distinction can facilitate the adaptation of the proposed method to varying operating conditions. Namely, the magnitude of the harmonic voltages for the compensation can be appropriately modulated through adjusting θ_t even if magnitude of the harmonic distortions from the inverter nonlinearity is changed due to altered operating conditions.

D. Modulation of the Compensation Voltage

The phase angle of the output current should be identified for the following reasons. The first reason is to synchronize the trapezoidal voltage with the output current, and the other is to modulate the trapezoidal angle. The a-phase angle, indicated by θ_a, can be selected as the phase angle, whose sine value, $\sin\theta_a$, is in phase with the a-phase output current. This phase angle can be simply obtained through the phase locked loop (PLL) [17]–[19]. Then, Park's transformation of (14) combined with (15) could be proceeded with respect to θ_a in order to modulate the trapezoidal angle

$$\begin{bmatrix} i_{ds}^a \\ i_{qs}^a \end{bmatrix} = \frac{2}{3} \cdot \begin{bmatrix} \cos\theta_a & \cos\theta_{a1} & \cos\theta_{a2} \\ -\sin\theta_a & -\sin\theta_{a1} & -\sin\theta_{a2} \end{bmatrix} \begin{bmatrix} i_{as} \\ i_{bs} \\ i_{cs} \end{bmatrix} \quad (14)$$

$$\theta_{a1} = \theta_a - \frac{2\pi}{3}, \quad \theta_{a2} = \theta_a + \frac{2\pi}{3} \quad (15)$$

where superscript "a" means that the d–q reference frame is synchronous with the a-phase angle.

The d-axis current in (14) can be especially useful to observe the harmonic currents. This is well exhibited with (17), which is derived from the insertion of (16) into (14)

$$\begin{cases} i_{as} = I_1 \cdot \sin\theta_a + I_5 \cdot \sin5\theta_a \\ i_{bs} = I_1 \cdot \sin\theta_{a1} + I_5 \cdot \sin5\theta_{a1} \\ i_{cs} = I_1 \cdot \sin\theta_{a2} + I_5 \cdot \sin5\theta_{a2} \end{cases} \quad (16)$$

$$\begin{cases} i_{ds}^a = I_5 \cdot \sin6\theta_a \\ i_{qs}^a = I_5 \cdot \cos6\theta_a - I_1 \end{cases} \quad (17)$$

where I_n is the magnitude of the nth-order harmonics.

The situation, where the fundamental currents are distorted by the fifth-order harmonics, is described in (16). If these currents are transformed into the d–q current by (14), only the harmonic component is observed in the d-axis whereas the fundamental one is also observed in the q-axis.

Meanwhile, when (17) is compared with (16), the magnitude of the harmonics is maintained, but the harmonic order is changed from fifth to sixth. A similar result can be deduced for the seventh-order harmonics. Namely, the magnitude of the harmonics is preserved, but the harmonic order is changed from seventh to sixth. Then, the fifth and seventh-order harmonics are transformed into the d-axis current like in

$$i_{ds}^a = (I_5 + I_7) \cdot \sin6\theta_a \quad (18)$$

where I_7 is the magnitude of the seventh-order harmonics.

The compensation is focused on the dominant harmonic, whose order is sixth in the synchronous d–q reference frame. The magnitude in (18) can be obtained with its polarity through signal processing as described in

$$\text{LPF}[i_{ds}^a \cdot \sin6\theta_a] \approx \frac{I_5 + I_7}{2} \quad (19)$$

where LPF stands for low-pass filtering of the signal.

The dc current, which is proportional to the magnitudes of the fifth- and seventh-order harmonic currents, can be obtained by the signal processing of (19). In particular, the polarity of the current obtained by (19) could be utilized to check whether the compensation for the fifth- and seventh-order harmonics is insufficient or excessive. Actual output currents are shown in Fig. 9 to demonstrate the relationship between the polarity and the compensation.

In Fig. 9(a), the output current i_{as} is clamped every zero-crossing. To prevent the clamping, more active support seems to be needed in the vicinity of the zero-crossing. This indicates that the compensation is insufficient. Under this condition, the output current can be transformed into the d-axis current, i_{ds}^a in Fig. 9(a). Since the main harmonic of the d-axis current is out of phase with $\sin6\theta_a$ in Fig. 9(a), the polarity by (19) would be negative.
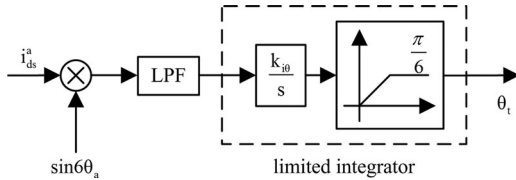
Fig. 10. Modulator for the trapezoidal angle.

Fig. 11. Conceptual circuit of the experimental setup.

Fig. 12. Test motor and inverter.

In Fig. 9(b), the output current is abruptly changed every zero-crossing. In this case, less active support seems to be needed in the vicinity of the zero-crossing. This means that the compensation is excessive. Under this condition, the main harmonic of the d-axis current is in phase with $\sin 6\theta_a$ as shown in Fig. 9(b). As a consequence, the polarity by (19) would be positive under the excessive compensation.

As described previously, the polarity by (19) can be utilized as the index indicating whether the compensation is insufficient or excessive. Using this index as the input to the limited integrator, a simple modulator could be designed to set the trapezoidal angle as shown in Fig. 10. Since the modulator output is just the angle, the relationship between the angle and compensation voltage also should be considered carefully.

As shown in Fig. 8, the magnitude of the fifth- and seventh-order harmonics monotonically decreased according to the increment of the angle up to 30°, which corresponds to $\pi/6$. This is why the integrator is limited in Fig. 10. Within the angle range, the harmonics of the compensation voltage could be simply adjusted through the modulator. For example, if the compensation is insufficient, the trapezoidal angle would be decreased by the integrator in Fig. 10, whose input would be negative as discussed in Fig. 9(a). As a result, the harmonics of the compensation voltage would be increased. In the opposite case, it is also correct for the angle to be changed according to the polarity by (19).

The current obtained by (19) may be neither positive nor negative. This means that the magnitudes of the harmonic currents are equal to zero. Moreover, the modulator output would converge on a certain value since the input to the integrator is zero. In a practical system, it is very difficult to perfectly eliminate the harmonic currents. However, the modulator output can almost settle down by the LPF of the integrator. Then, under certain operating conditions, varying the trapezoidal angle would be stopped when the harmonic currents almost disappear or the limiter of the integrator operates. And, if the change under the operating condition causes more harmonic currents, the trapezoidal angle would be adjusted into another angle toward minimizing the harmonic currents. All of these adaptations could be achieved with the simple modulator in Fig. 10 without the aid of any observers. The integral gain of the modulator, $k_{i\theta}$ in Fig. 10, was empirically set as 20 for the practical system specified in Section III-A within the entire operating range.

III. EXPERIMENTS

A. Experimental Setup

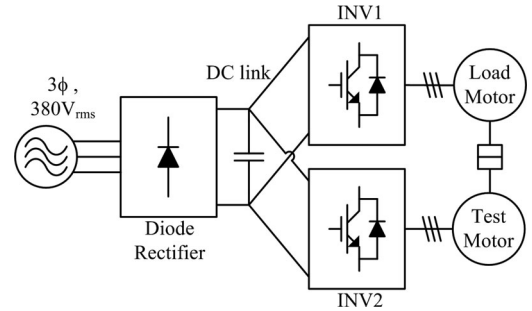The concept of the experimental setup is depicted in Fig. 11. Two motors were coupled to each other mechanically, and both inverters shared the dc link, which came from a 3ϕ-380 $V_{\rm rms}$ voltage source via the diode rectifier. Insulated gate bipolar transistor (IGBT) modules, 75 A 1200 V, were used as the power semiconductors of the inverters.
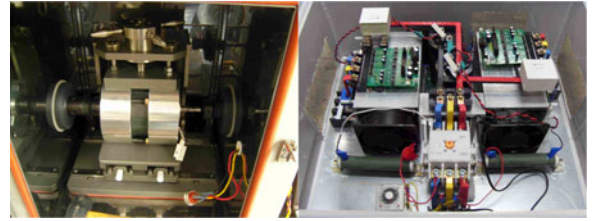
The motor under test was a 6.8-kW interior permanent magnet synchronous motor (IPMSM) shown in Fig. 12, and controlled with the sensorless method in [1]. The load motor was controlled with a resolver to apply the load torque to the motor under test.

A control board based on the DSP, TMS320VC33, was used to generate switching signals of the IGBT modules. Furthermore, all control algorithms are implemented digitally with the DSP board. The periods of sampling and switching were, respectively, selected as 100 and 200 μs. This means 5-kHz switching and double sampling in a switching period. In addition, the preset dead time was 3 μs.

B. Purpose of the Experiments

The effectiveness of the proposed compensation method was examined through comparisons with other previously published compensation methods, which are described in [4] and [5], because they are based on the same information with the proposed method shown in Fig. 6. For convenience, the method in [4] was designated as the "square method" since its compensation voltage is a square wave. Additionally, the method in [5] was designated as the "table method," in which a look-up table is used for the compensation.

First, the output current of each compensation method was compared. Harmonics are not desirable in the line current to the PMSM because it means additional Ohmic losses and torque ripples. Therefore, it is informative to evaluate each method to determine to what degree the harmonics in the current are mitigated.

As mentioned before, inverter nonlinearity indicates the differences between the voltage references and actual outputs. For
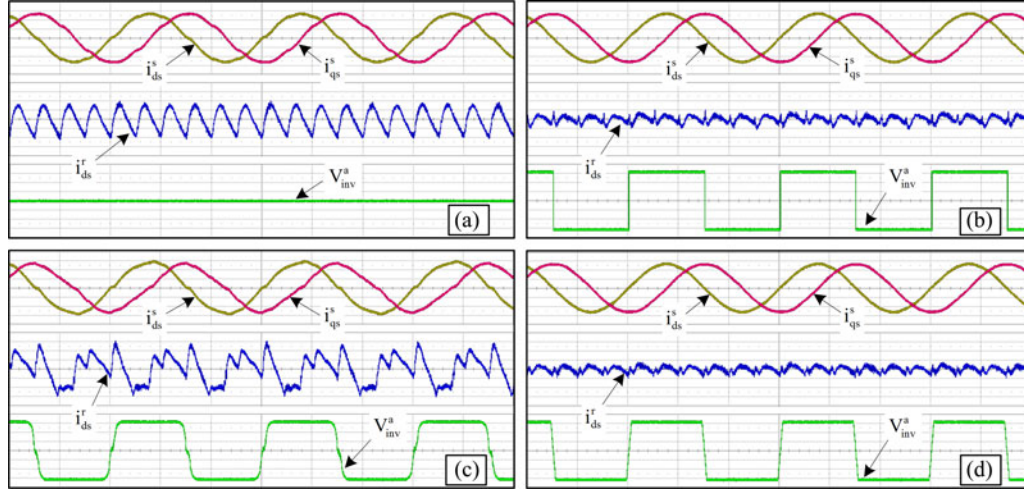
Fig. 13. Output current and compensation voltage, 500 r/min, 4 N-m load: (a) no compensation, (b) square method, (c) table method, and (d) proposed method: i_{ds}^s, i_{qs}^s (3 A/div, center 0 A), i_{ds}^r (0.25 A/div, center 0 A), V_{inv}^a (2.5 V/div, center 0 V), time (20 ms/div).

a balanced motor-load, balanced voltage references should be observed if the nonlinearity is perfectly eliminated. Then, how much the voltage references resemble a balanced three-phase wave could also be used as an effectiveness index to compare the compensation methods.

In addition, it would allow us to investigate how the sensor-less control system is affected by the compensation since the harmonic distortions can also be reflected by the estimation of the rotor angle and rotating speed.

C. Experimental Results

Basically, i_{ds}^r, whose superscript "r" indicates the rotor d–q reference frame, was regulated as zero for simplicity. The motor was operated with a 4 N-m load at 500 r/min for the first comparison. The compensation results from each method are shown in Fig. 13. From the figure, it is clear which part is similar to or different from each other. To evaluate the effectiveness, conspicuous comparisons were possible for i_{ds}^r rather than for i_{ds}^s or i_{qs}^s. The q-axis current in the rotor reference frame was not displayed because the magnitudes of the harmonic currents were the same in the d- and q-axis as derived in (17).

Compared to the case with no compensation, the harmonics were evidently mitigated by the proposed method shown in Fig. 13(d). For the table method, although the compensation voltage V_{inv}^a resembles a trapezoid, the resultant harmonics were very different from those of the proposed method. This can be regarded as the indirect example caused by an unsuitable trapezoidal angle. The data stored in the table may only be effective under certain operating conditions.

However, the square method also had an excellent result shown in Fig. 13(b). This is because the effect of the parasitic capacitances was not dominant under the test condition, where the magnitude and frequency of the output current are large enough. Namely, the square method can be analogous with the proposed method if the parasitic capacitances are negligible.

To differentiate the square and proposed methods, the motor under test was driven at 150 r/min with no load in the experi-

ments of Fig. 14. Both the magnitude and frequency of the line current to the PMSM were small enough under this operating condition. As the result, the square method was not effective any more shown in Fig. 14(b) whereas the proposed method was still effective. Rather, the current harmonics increased more by the square method compared to the case with no compensation.

In Fig. 14, the proposed method still exhibited its effectiveness and was superior to the other compensation methods. However, it seems that the harmonics of i_{ds}^r in Fig. 14(d) were not reduced much compared to the case with no compensation due to the sampling noises. Hence, i_{ds}^s and i_{qs}^s were used for fast Fourier transform (FFT) analyses to quantify the compensation results. The data for FFT were sampled for 5000 s with 1000 sample/s, and the frequency of the output current was 5 Hz.

The FFT results are shown in Fig. 15 for the currents in Fig. 14(a) and (d), and the ratio of each harmonic to the fundamental is summarized in Table I. Although the harmonics of the 11th and 13th slightly increased, the main harmonics of the 5th and 7th decreased conspicuously by the proposed method. A selective harmonic distortions (SHD) could be defined as in

$$\text{SHD}[\%] = \frac{\sqrt{I_5^2 + I_7^2 + I_{11}^2 + I_{13}^2}}{I_1} \times 100 \qquad (20)$$

where I_k is the magnitude of the kth-order harmonic.

If the magnitude of each harmonic is inserted into (20), the SHDs of the d- and q-axis currents in Fig. 15(a) are calculated as 7.1% and 7.22%, and 2.29% and 2.4% in Fig. 15(b), respectively. Therefore, based on the SHDs, it is concluded that the harmonic distortions decreased by about 67% in the output currents with the proposed compensation method.

In addition to the output current, the voltage references could also be used for the evaluation. The motor was driven under the same condition as in the experiments of Fig. 14. For each compensation method, the voltage references in the stationary d–q reference frame are shown in Fig. 16.

As mentioned in the previous section, the voltage references should be a balanced three-phase wave without any distortions
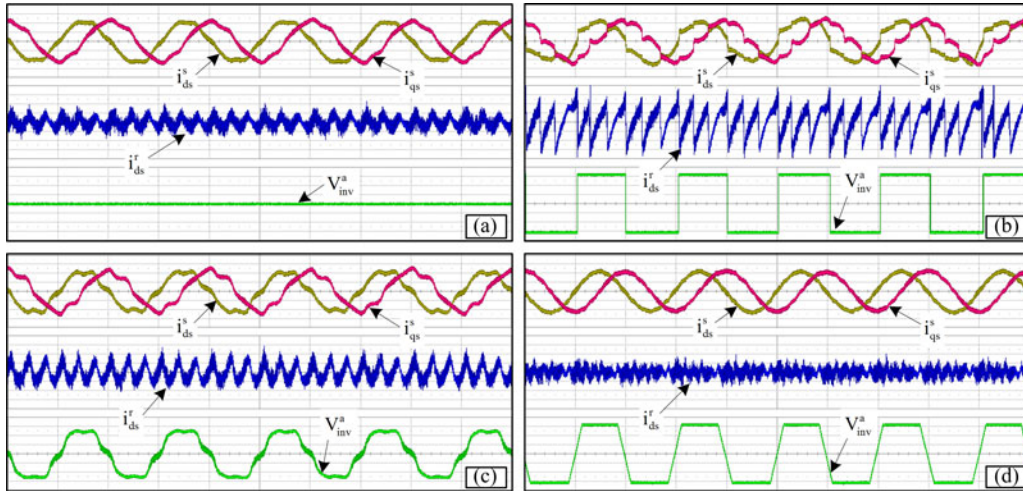
Fig. 14.   Output current and compensation voltage, 150 r/min, no load: (a) no compensation, (b) square method, (c) table method, (d) proposed method: i_{ds}^s, i_{qs}^s (0.5 A/div, center 0 A), i_{ds}^r (0.1 A/div, center 0 A), V_{inv}^a (2.5 V/div, center 0 V), time (100 ms/div).
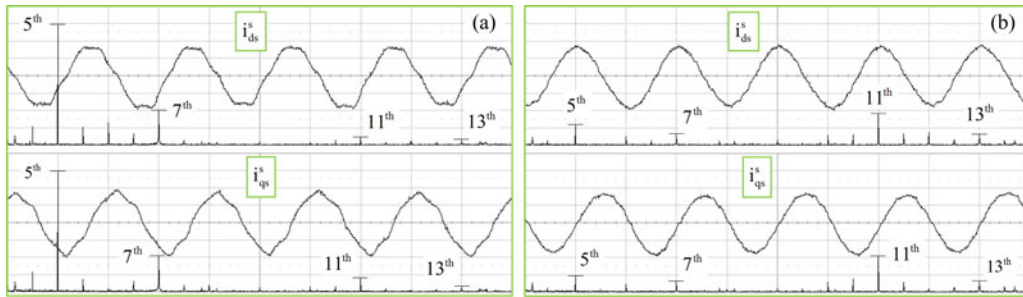

Fig. 15.   FFT results for output currents, 150 r/min, no load: (a) no compensation, (b) proposed method: i_{ds}^s, i_{qs}^s (0.6 A/div, center 0 A), time (100 ms/div), FFT currents (9.6 mA/div, center 38.4 mA), frequency (5 Hz/div, center 45 Hz).

TABLE I
FFT RESULTS FOR THE OUTPUT CURRENT IN FIG. 15

		Ratio to the fundamental [%]	
		No compensation	Proposed method
i_{ds}^s	5th	6.81	1.128
	7th	1.94	0.628
	11th	0.426	1.798
	13th	0.277	0.575
i_{qs}^s	5th	6.88	0.906
	7th	2.04	0.586
	11th	0.76	2.06
	13th	0.278	0.62

if the nonlinearity is totally eliminated from the inverter under the test. The three-phase voltage should be pure sine waves in the stationary d–q reference frame. As shown in Fig. 16, the voltage references were the closest to the ideal case with the proposed method. This result also demonstrates the superiority of the proposed method.

Besides the harmonic distortions, the fundamentals of the voltage references also decreased by the proposed method compared to the case with no compensation in Fig. 16. This is because the trapezoidal voltage includes a component whose frequency coincides with the fundamental frequency. The fundamental component of the compensation voltage is mainly determined by V_{sat} in Fig. 6, and its variation is limited to less

than 4.5% during the compensation as described in Section II-C. This property is different from the compensation itself, which uses a dedicated controller at a specified harmonic frequency. Compensating for the fundamental distortion could be useful for the parameter estimations of a drive system, where the voltage references are used instead of the actual voltage outputs [20].

Actually, the voltage distortions in Fig. 16 may be intensified by the actions of the sensorless control system. As shown in Fig. 16, the estimated speed $\hat{\omega}_{rpm}$ is different from the actual speed ω_{rpm}, which is measured through the resolver. This is because voltage references are used to estimate the speed. Namely, the harmonics in the voltage references are reflected in the speed estimation. Since the estimated speed is used for the speed control in the sensorless control system, the harmonics in the speed affects the current references. Moreover, the rotor angle, used for the current control, also includes the same harmonics since the angle is the integral of the speed. Eventually, the distortions are fed back to the voltage references through the current references. Therefore, it is more effective to suppress the origin of the harmonics through the compensation.

For the compensation combined with a sensorless control system, the overall performance can be evaluated based on all the results in Figs. 13–16. If the compensation is not proper, the harmonic distortions are not only limited to the currents, but also can be spread and amplified through the control loop of the
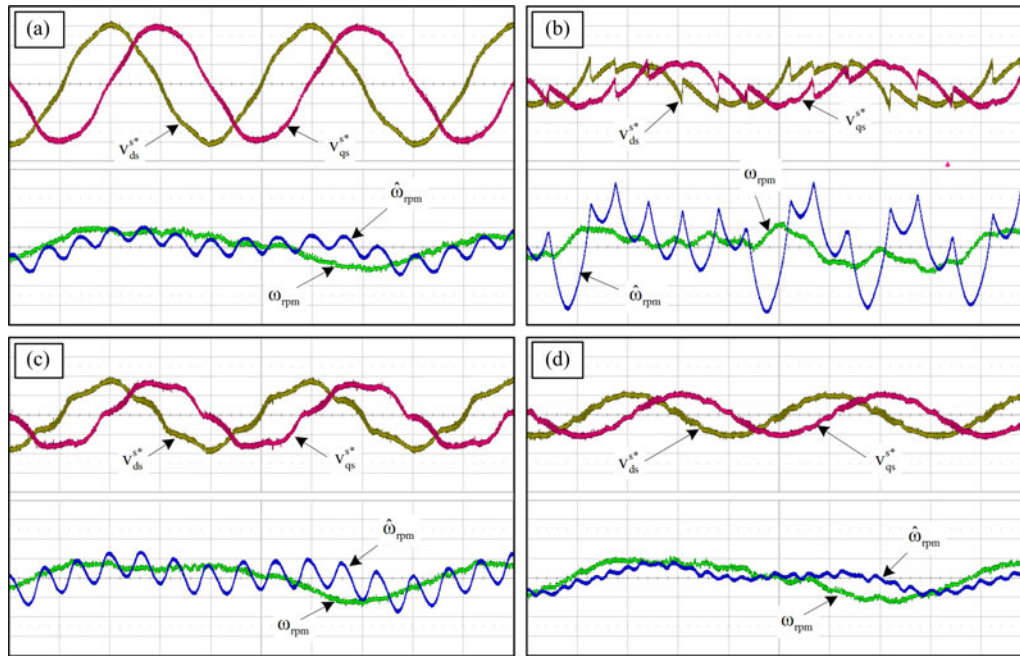
Fig. 16. Voltage references, actual speed, and estimated speed, 150 r/min, no load: (a) no compensation, (b) square method, (c) table method, and (d) proposed method: v_{ds}^{s*}, v_{qs}^{s*} (5 V/div, center 0 V), $\omega_{\rm rpm}$, $\hat{\omega}_{\rm rpm}$ (5 r/min/div, center 150 r/min), time (50 ms/div).

system shown in Fig. 16(b), where the harmonics are reflected even on the actual speed in contrast to the others. That is, torque ripples can be generated by itself even in a steady state.

As shown in Figs. 13–16, all distortions clearly had been mitigated by the proposed method in the current, voltage, and speed. This is because the compensation voltages were modified in real time and adapted to various operating conditions. The performance of the sensorless control system can be enhanced by the proposed method.

IV. CONCLUSION

In this paper, a novel method was proposed to compensate for inverter nonlinearity. Basically, the proposed method could be applied to a control system with a position sensor for driving a PMSM. However, a sensorless control system with the PMSM was selected to demonstrate the proposed method in order to consider more diverse effects from the nonlinearity.

To achieve the compensation in the software stage, the nonlinearity was considered as the distorted voltage per one sampling period. Trapezoidal voltage was exploited to compensate for the distorted voltage since the harmonic voltages in the trapezoid can be controlled through the trapezoidal angle. The integral controller was utilized to find a suitable trapezoidal angle in real time with signal processing.

The effectiveness of the proposed method was discussed through comparisons with conventional methods. Experimental results under several operating conditions showed that the harmonic distortions are suppressed conspicuously in the overall system by the proposed method. Contrary to the other methods, the proposed method maintained its effectiveness under various operating conditions.

REFERENCES

[1] B.-H. Bae, S.-K. Sul, J.-H. Kwon, and J.-S. Byeon, "Implementation of sensorless vector control for super-high speed PMSM of turbo-compressor," *IEEE Trans. Ind. Appl.*, vol. 39, no. 3, pp. 811–818, May/Jun. 2003.

[2] S. Morimoto, K. Kawamoto, M. Sanada, and Y. Takeda, "Sensorless control strategy for salient-pole PMSM based on extended EMF in rotating reference frame," *IEEE Trans. Ind. Appl.*, vol. 38, no. 4, pp. 1054–1061, Jul./Aug. 2002.

[3] B. Nahid-Mobarakeh, F. Meibody-Tabar, and F.-M. Sargos, "Back EMF estimation-based sensorless control of PMSM: Robustness with respect to measurement errors and inverter irregularities," *IEEE Trans. Ind. Appl.*, vol. 43, no. 2, pp. 485–494, Mar./Apr. 2007.

[4] J.-W. Choi and S.-K. Sul, "Inverter output voltage synthesis using novel dead time compensation," *IEEE Trans. Power Electron.*, vol. 11, no. 2, pp. 221–227, Mar. 1996.

[5] G. Pellegrino, R. I. Bojoi, P. Guglielmi, and F. Cupertino, "Accurate inverter error compensation and related self-commissioning scheme in sensorless induction motor drives," *IEEE Trans. Ind. Appl.*, vol. 46, no. 5, pp. 1970–1978, Sep./Oct. 2010.

[6] J.-W. Choi and S.-K. Sul, "A new compensation strategy reducing voltage/current distortion in PWM VSI systems operating with low output voltages," *IEEE Trans. Ind. Appl.*, vol. 31, no. 5, pp. 1001–1008, Sep./Oct. 1995.

[7] N. Urasaki, T. Senjyu, T. Kinjo, T. Funabashi, and H. Sekine, "Dead-time compensation for permanent magnet synchronous motor drive taking zero-current clamp and parasitic capacitance effects into account," *IEE Proc. Electric Power Appl.*, vol. 152, no. 4, pp. 845–853, Jul. 2005.

[8] D. Leggate and R. J. Kerkman, "Pulse-based dead-time compensator for PWM voltage inverters," *IEEE Trans. Ind. Electron.*, vol. 44, no. 2, pp. 191–197, Apr. 1997.

[9] A. R. Munoz and T. A. Lipo, "On-line dead-time compensation technique for open-loop PWM-VSI drives," *IEEE Trans. Power Electron.*, vol. 14, no. 4, pp. 683–689, Jul. 1999.

[10] L. Chen and F. Z. Peng, "Dead-time elimination for voltage source inverters," *IEEE Trans. Power Electron.*, vol. 23, no. 2, pp. 574–580, Mar. 2008.

[11] T. Itkonen, J. Luukko, A. Sankala, T. Laakkonen, and R. Pollanen, "Modeling and analysis of the dead-time effects in parallel PWM two-level three-phase voltage-source inverter," *IEEE Trans. Power Electron.*, vol. 24, no. 11, pp. 2446–2455, Nov. 2009.

[12] L. M. Gong and Z. Q. Zhu, "Modeling and compensation of inverter nonlinearity effects in carrier signal injection-based sensorless control methods from positive sequence carrier current distortion," in *Proc. IEEE Energy Convers. Congr. Exposition*, Sep.12–16, 2010, pp. 3434–3441.

[13] T. Hoshino and J.-I. Itoh, "Output voltage correction for a voltage source type inverter of an induction motor drive," *IEEE Trans. Power Electron.*, vol. 25, no. 9, pp. 2440–2449, Sep. 2010.

[14] S.-Y. Kim, W. Lee, M.-S. Rho, and S.-Y. Park, "Effective dead-time compensation using a simple vectorial disturbance estimator in PMSM drives," *IEEE Trans. Ind. Electron.*, vol. 57, no. 5, pp. 1609–1614, May 2010.

[15] S.-H. Hwang and J.-M. Kim, "Dead time compensation method for voltage-fed PWM inverter," *IEEE Trans. Energy Convers.*, vol. 25, no. 1, pp. 1–10, Mar. 2010.

[16] H.-S. Kim, H.-T. Moon, and M.-J. Youn, "On-line dead-time compensation method using disturbance observer," *IEEE Trans. Power Electron.*, vol. 18, no. 6, pp. 1336–1345, Nov. 2003.

[17] S. Bolognani, L. Pretti, and M. Zigliotto, "Repetitive-control -based self-commissioning procedure for inverter nonidealities compensation," *IEEE Trans. Ind. Appl.*, vol. 44, no. 5, pp. 1587–1596, Sep./Oct. 2008.

[18] Y. F. Wang and Y. W. Li, "Analysis and digital implementation of cascaded delayed-signal-cancellation PLL," *IEEE Trans. Power Electron.*, vol. 26, no. 4, pp. 1067–1080, Apr. 2011.

[19] F. D. Jreijedo, A. G. Yepes, O. Lopez, A. Vidal, and J. Doval-Gandoy, "Three-phase PLLs with fast postfault retracking and steady-state rejection of voltage unbalance and harmonics by means of lead compensation," *IEEE Trans. Power Electron.*, vol. 25, no. 1, pp. 85–97, Jan. 2011.

[20] Y. Inoue, K. Yamada, S. Morimoto, and M. Sanada, "Effectiveness of voltage error compensation and parameter identification for model-based sensorless control of IPMSM," *IEEE Trans. Ind. Appl.*, vol. 45, no. 1, pp. 213–221, Jan./Feb. 2009.

Yongsoon Park (S'12) received the B.S. and M.S. degrees in electrical engineering from Seoul National University, Seoul, Korea, in 2008 and 2010, respectively, where he is currently working toward the Ph.D. degree.

His current research interests include sensorless drives of electrical machines and power conversion circuits.

Seung-Ki Sul (S'78–M'80–SM'98–F'00) received the B.S, M.S, and Ph.D. degrees in electrical engineering from Seoul National University, Seoul, Korea, in 1980, 1983, and 1986, respectively.

From 1986 to 1988, he was an Associate Researcher in the Department of Electrical and Computer Engineering, University of Wisconsin, Madison. From 1988 to 1990, he was a Principal Research Engineer with Gold-Star Industrial Systems Company. Since 1991, he has been a member of the faculty of the School of Electrical Engineering, Seoul National University, where he is currently a Professor. From 2005 to 2007, he was the Vice Dean of Electrical Engineering, Seoul National University. From 2008 to 2011, he was the President of Korea Electrical Engineering and Science Research Institute. His current research interests include power electronic control of electrical machines, electric/hybrid vehicle and ship drives, and power-converter circuits.